Quantitative Evaluation of Type 1 and Type 2 Choroidal Neovascularization Components Under Treatment With Projection-Resolved OCT Angiography

Kotaro Tsuboi,[1,2] Qi Sheng You,[1] Jie Wang,[1,3] Yukun Guo,[3] Christina J. Flaxel,[1] Thomas S. Hwang,[1] David Huang,[1,3] Yali Jia,[1,3] and Steven T. Bailey[1]

[1]Casey Eye Institute, Oregon Health & Science University, Portland, Oregon, United States
[2]Department of Ophthalmology, Aichi Medical University, Nagakute, Japan
[3]Department of Biomedical Engineering, Oregon Health & Science University, Portland, Oregon, United States

Correspondence: Steven T. Bailey, Casey Eye Institute, Oregon Health & Science University, 515 SW Campus Drive, Portland, OR 97239, USA;
bailstev@ohsu.edu.

Received: January 3, 2024
Accepted: September 1, 2024
Published: September 20, 2024

Citation: Tsuboi K, You QS, Wang J, et al. Quantitative evaluation of type 1 and type 2 choroidal neovascularization components under treatment with projection-resolved OCT angiography. *Invest Ophthalmol Vis Sci.* 2024;65(11):32.
https://doi.org/10.1167/iovs.65.11.32

Purpose. To evaluate the response of type 1 and type 2 macular neovascularization (MNV) components under anti-vascular endothelial growth factor (VEGF) treatment in age-related macular degeneration (AMD) using projection-resolved optical coherence tomography angiography (PR-OCTA).

Methods. This retrospective study included eyes with treatment-naïve exudative AMD treated with anti-VEGF injections under a pro re nata (PRN) protocol over 1 year. Two-dimensional MNV areas and three-dimensional MNV volumes were derived from macular PR-OCTA scans using an automated convolutional neural network. MNV was detected as flow signal within the outer retinal slab. Type 1 components and type 2 components were analyzed separately.

Results. Of 17 enrolled eyes, 12 eyes were pure type 1 MNV and five eyes were type 2 MNV. In eyes with pure type 1, the total (sum of type 1 and type 2 components) MNV area and volume did not change from baseline to 6 months or 12 months ($P > 0.05$). In eyes with type 2 MNV, the total MNV area significantly decreased from the baseline to 6 months ($P = 0.0074$) and 12 months ($P = 0.014$). The total type 2 MNV volume also decreased from baseline visit to visits at 6 months and at 12 months, nearing statistical signifiicance ($P = 0.061$ and $P = 0.074$). In eyes with type 2 MNV, the type 1 component increased from 0.093 mm^2 to 0.30 mm^2 ($P = 0.058$), and the type 2 component decreased from 0.37 mm^2 at 6 months to 0 at 12 months ($P = 0.0087$).

Conclusions. Type 1 and type 2 MNV may have different response under PRN anti-VEGF treatment over 1 year.

Keywords: OCTA, CNV, CNN-based algorithm

Age-related macular degeneration (AMD) is a leading cause of vision loss and irreversible blindness.[1,2] Exudative AMD accounts for most vision loss and is characterized by the formation of macular neovascularization (MNV), formerly referred to as choroidal neovascularization (CNV).[3–5] The first official classification of exudative AMD was established in 1991 by the Macula Photocoagulation Study.[6] With this fluorescein angiography (FA)-based classification, classic CNV and occult CNV were defined based on the hyperfluorescent patterns. Another classification, first proposed by Gass,[7] was two types of CNV based on the location of the neovascular complex with respect to the retinal pigment epithelial (RPE). This histopathologic study provided the description as type 1 CNV, which is below the RPE, or type 2 CNV, which extends within the subretinal space. Optical coherence tomography (OCT) allowed us to classify histologic description in vivo[8]; however, OCT-based classification lacked the three-dimensional and vascular information.

Optical coherence tomography angiography (OCTA) provides a three-dimensional and quantitative assessment of the retinal and choroidal vasculature.[9,10] The projection-resolved (PR) algorithm also improves the depth resolution and image quality of pathologic blood flow in the outer retina,[11,12] enhancing both cross-sectional and en face visualization of MNV.[13,14] However, quantitative analysis of MNV remains difficult even with PR-OCTA due to the residual artifacts.[15] Recently, we have developed a fully automated MNV diagnosis and segmentation algorithm using convolutional neural networks (CNNs).[16,17] This algorithm has improved MNV diagnosis accuracy and MNV membrane segmentation, enabling quantification of distinct MNV components, type 1 and type 2.[13] The combination of PR-OCTA with the CNN algorithm allows for separate quantitative analysis of MNV type 1 and type 2 components.

Prior studies using FA and OCT have reported that different MNV types (classic and occult, or type 1 and type 2) have different treatment responses under anti-vascular endothelial growth factor (VEGF) treatment.[18,19] Studies using OCTA have also demonstrated different responses to anti-VEGF treatment depending on the type of MNV.[20–23] However, these studies analyzed both type 1 and type 2 MNV compo-

nents at the same time. Because type 1 and type 2 MNV components sometimes coexist and MNV is often multilayered on OCTA,[21,24,25] analyzing type 1 MNV and type 2 MNV components separately is important for precise analysis. In the current study, we applied the novel CNN algorithm on eyes with treatment-naïve exudative AMD under a pro re nata (PRN) anti-VEGF injection protocol that lasted 1 year in duration. The aim of this study was to evaluate the quantitative changes of individual MNV components, type 1 and type 2, under PRN anti-VEGF treatment over 1 year.

Methods

Study Population

This was a retrospective secondary analysis study using data obtained from a prospective study evaluating the role of OCTA in neovascular AMD (National Eye Institute, National Institutes of Health, R01EY024544-01) and was performed at the Casey Eye Institute, Oregon Health & Science University. Study participants were recruited from the retina clinics at the Casey Eye Institute from September 2014 through November 2018. Consecutive patients with treatment-naïve neovascular AMD were enrolled to participate in the PRN anti-VEGF treatment protocol requiring monthly visits for 1 year. The treating physician and patient selected the anti-VEGF agent of their choice. Treatment was provided if intra- or subretinal fluid was identified on 19 slices of cross-sectional OCT images captured by spectral-domain OCT (SD-OCT; SPECTRALIS; Heidelberg Engineering, Heidelberg, Germany) or if there was subretinal hemorrhage on clinical exam. This study focused on type 1 and type 2 MNV, and cases of type 3 MNV were excluded. Other exclusion criteria were poor OCTA image quality with shadow and motion artifacts and signal strength index (SSI) < 45, as well as patients with any other macular disease such as an epiretinal membrane or vitreomacular traction syndrome and refractive error greater than -6 or $+3$ diopters. This study was conducted with the informed consent of patients, in accordance with the tenets of the Declaration of Helsinki and with the approval of the Oregon Health & Science University institutional review board.

General Examinations

Examinations performed at baseline included visual acuity using the Early Treatment Diabetic Retinopathy Study (ETDRS) chart, intraocular pressure, slit lamp, dilated fundus, axial length measurement (ZEISS IOLMaster 500; Carl Zeiss Meditec, Jena, Germany), structural SD-OCT (Heidelberg SPECTRALIS), FA, and OCTA. Central subfield thickness (CST), an average retinal thickness within a 1-mm circle centered on the fovea, was assessed with the SPECTRALIS. Each of these evaluations, except for axial length measurement and FA, was repeated at 6- and 12-month visits. FA was performed at the baseline visit to confirm the presence of MNV. Retinal specialists (KT, SB) reviewed all cases and excluded type 3 MNV at baseline for exclusion and determined if RPE envelopment developed during the follow-up period.

OCTA Acquisition and Processing

OCTA scans were acquired using commercially available SD-OCT (RTVue XR OCT Avanti with AngioVue Software; Optovue, Fremont, CA, USA) with a center wavelength of 840 nm and 70-kHz axial scan rate. Both 3×3-mm and 6×6-mm OCTA scans centered on the macula were obtained for each study eye at each visit. We preferentially selected 3×3-mm scan patterns for analysis; however, if MNV extended beyond the 3×3-mm field of view, then 6×6-mm OCTA angiograms were used to capture the entire MNV. The scan pattern used for the baseline visit was used for the analysis for all subsequent follow-up visits to ensure consistency in the analysis over the course of the study. Angiograms were exported to the Casey Eye Reading Center for custom processing using Center for Ophthalmic Optics & Lasers Angiography Reading Toolkit (COOL-ART) software. A semi-automated algorithm based on a directional graph search segmented the volumes.[26] Segmentations were then reviewed and manually adjusted to ensure accuracy by two graders (KT, JW). MNV was detected in the outer retinal slab, which is between the outer boundary of the outer plexiform layer and Bruch's membrane.

Automated MNV Area and Volume Measurements

The MNV area was measured using a CNN, as previously reported.[16,17] Briefly, this automated segmentation of the MNV algorithm was trained by a clinical dataset, including both scans with and without MNV. The study results showed good MNV segmentation accuracy compared to the ground truth with the mean intersection over a union of 0.88. In the current study, we used this algorithm to measure MNV lesions as MNV area. We separately measured the type 1 component and type 2 component based on the segmentation of the RPE, which was manually verified and adjusted if needed. A total MNV area was defined as the sum of type 1 and type 2 components. If an RPE envelopment covering type 2 MNV occurred during the follow-up, that type 2 MNV component was included in the type 1 MNV component. MNV volume was defined as the volumetric flow signals between the outer boundary of the outer plexiform layer and Bruch's membrane (Supplementary Video S1). MNV volume was separated into type 1 and type 2 components as either above or below the RPE, respectively. The area and volume of MNV measurements were corrected for axial length–related magnification using the axial length with Bennett formula.[27]

MNV types were subdivided based on MNV area measured by OCTA as previously reported[13]—namely, pure type 1 MNV is when 100% of the MNV area is below the RPE; predominantly type 2 MNV is when >75% of the total MNV area is above the RPE; and the mixed type occurs when the type 1 area is greater than 25% of the total MNV area and there is a type 2 MNV area, as well (Fig. 1).

Statistical Analysis

The data are expressed as mean, standard deviation (SD), and range, as appropriate. We used one-way repeated-measures analysis of variance (ANOVA) and paired *t*-test or Friedman test and Wilcoxon signed-rank test to assess longitudinal 1-year changes in MNV area and volume. We compared the relationship between MNV area and MNV volume with Spearman's rank correlation coefficient. To compare eyes with pure type 1 MNV and type 2 MNV, interaction terms between time (from baseline to 12 months) and parameters (pure type 1 MNV or type 2 MNV) were included as fixed effects in these models, and the subjects were

Investigative Ophthalmology & Visual Science

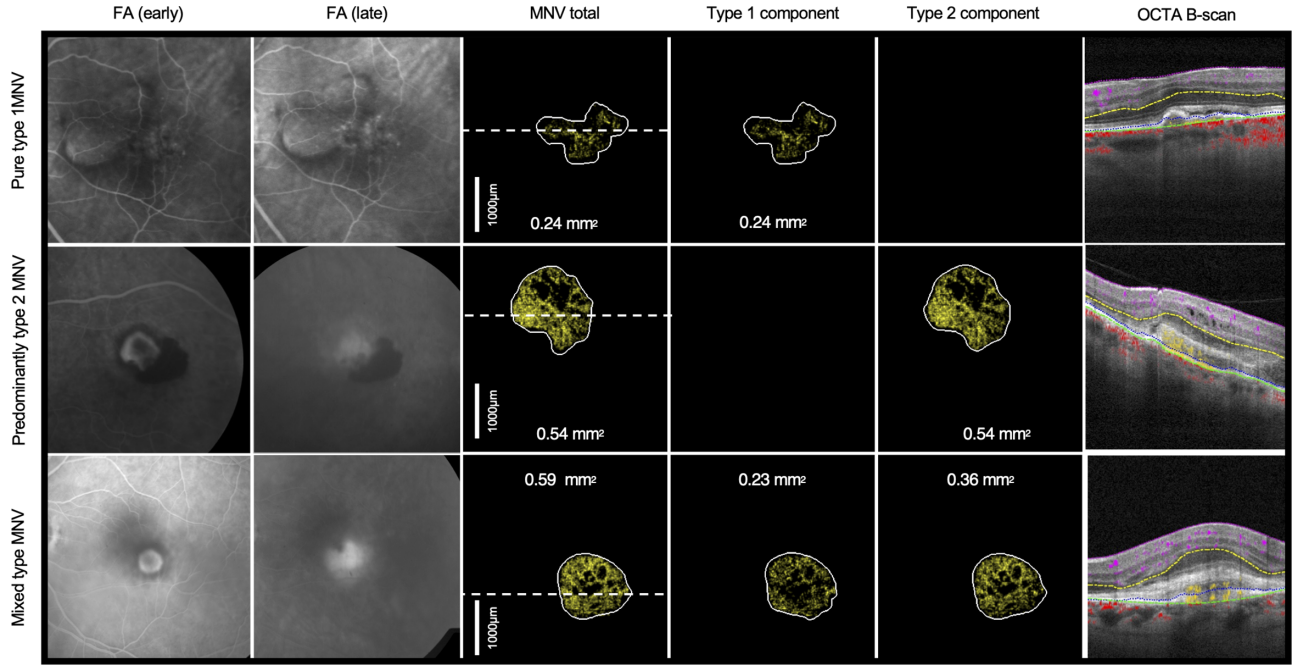

Figure 1. Representative examples of MNV type based on OCTA-based classification and corresponding early and late FA. Total area, type 1 MNV area, and type 2 MNV area were detected with automated MNV lesion measurement.

included as random effects. The model was adjusted by the number of anti-VEGF injections over 6 months or 12 months. All analyses were done using JMP 13.1.0 (SAS Institute, Cary, NC, USA) and Prism (GraphPad, Boston, MA, USA). $P < 0.05$ was considered statistically significant. When we performed multiple comparisons, the significance level (P value) was adjusted using the Bonferroni correction method.

Results

Initially, 27 eyes from 25 study participants with treatment-naïve exudative AMD were enrolled in this study. In eight eyes (30%), MNV was detected but low image quality prevented quantification. Two eyes (7%) were also excluded due to the presence of type 3 macular neovascularization. Finally, 17 eyes from 15 study participants were included in this study. Fourteen patients (93%) were female, and the mean (SD) age was 76 (9). The mean ± SD ETDRS letter score was 70.9 ± 13.7, and the mean CST was 344 ± 85 μm at the baseline. A 3 × 3-mm scan area was used for 12 eyes, and a 6 × 6-mm scan area was used for five eyes. There were no differences in SSI between visits ($P > 0.05$). Patient characteristics are summarized in Table 1. Five eyes (39%) were classified as classic with FA, and each of these was graded as type 2 MNV with OCTA. The remaining 12 eyes (71%) were graded as occult with FA, and each of these was graded as type 1 MNV with OCTA. The mean number of visits was 12.6 ± 0.8, which means that 13 eyes (76%) completed monthly visits over the 1-year follow-up. The mean total number of anti-VEGF injections during 1-year follow-up was 8.8 ± 4.4.

Table 1. Baseline and 12-Month Parameters Among MNV Types at Baseline

	Mean (SD)			
Parameter	**All Eyes (n = 17)**	**Pure Type 1 MNV (n = 12)**	**Type 2 MNV (n = 5)**	***P***
Baseline visual acuity (ETDRS letter score)	70.9 (13.7) [63.9 to 77.9]	73.6 (11.5) [66.3 to 80.9]	64.4 (17.7) [42.4 to 88.4]	0.33
Baseline CST (μm)	344 (85) [300.3 to 388.0]	309.3 (52.6) [276.4 to 343.3]	426.4 (97.5) [305.4 to 547.4]	0.053
12-Month visual acuity (ETDRS letter score)	73.9 (10.9) [68.4 to 79.5]	74.4 (8.7) [68.9 to 80.0]	72.8 (16.2) [52.7 to 92.9]	0.84
12-Month CST (μm)	295 (51) [268.7 to 321.2]	292.2 (54.9) [257.3 to 327.0]	301.6 (45.9) [244.6 to 358.6]	0.72
Total number of anti-VEGF injections	8.8 (4.4) [6.5 to 11.0]	8.4 (4.6) [5.5 to 11.4]	9.6 (4.3) [4.3 to 14.9]	0.42
Total number of visits	12.6 (0.8)	12.6 (0.8) [12.1 to 13.1]	12.6 (0.9) [11.5 to 13.7]	0.89
Baseline SSI	58.0 (7.2) [54.3 to 61.7]	—	—	—
6-Month SSI	59.2 (8.0) [55.1 to 63.3]	—	—	—
12-Month SSI	60.0 (7.6) [56.1 to 63.9]	—	—	—
1-Year change in visual acuity (ETDRS letter score)	3.1 (8.3) [−1.2 to 7.3]	0.8 (6.8) [−3.5 to 5.1]	8.4 (9.9) [−3.9 to 20.7]	0.17
1-Year change in CST (μm)	−49.2 (87.0) [−93.9 to −4.5]	−17.7 (68.7) [−61.2 to 26.0]	−124.8 (84.7) [−230 to −19.6]	0.044

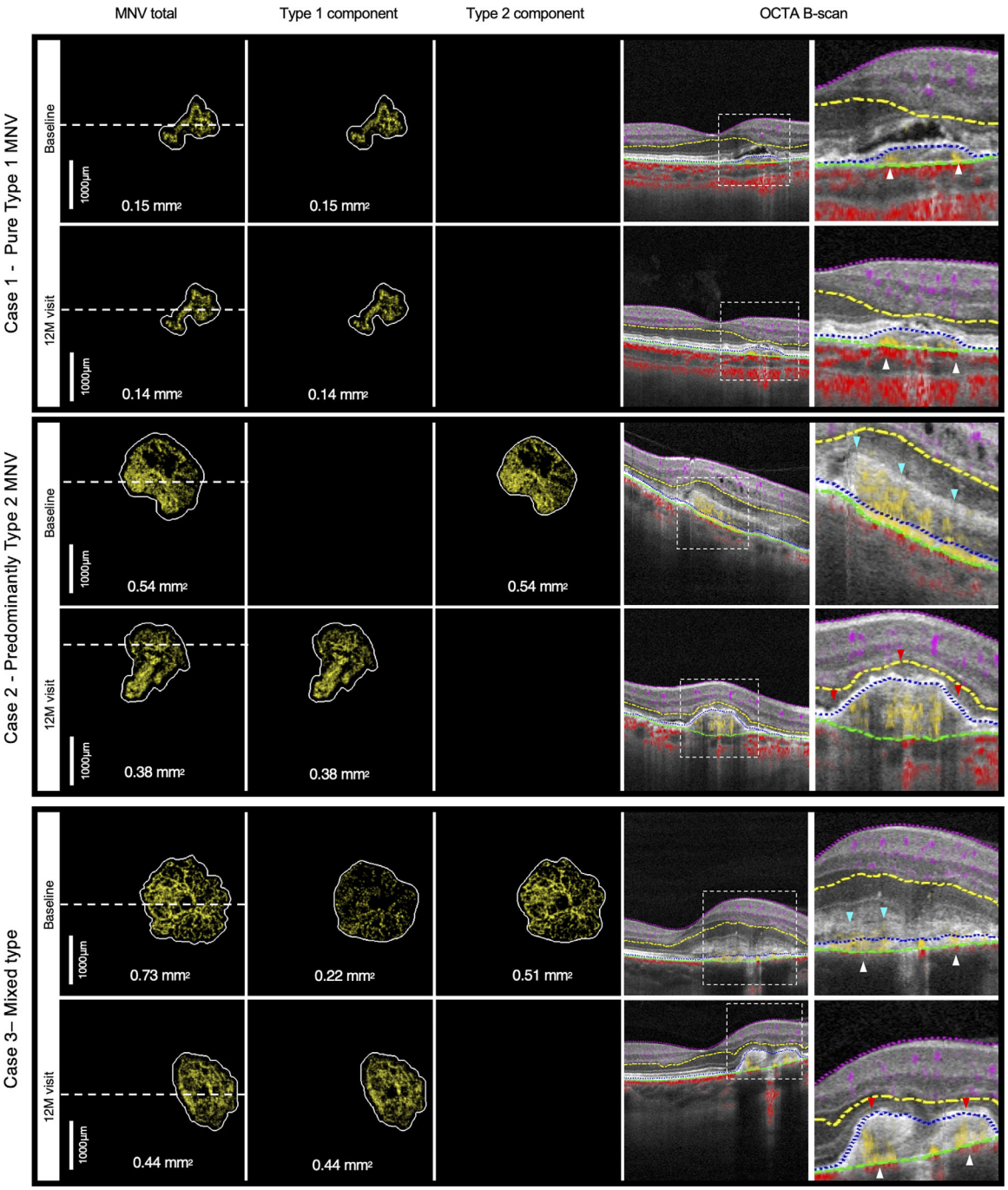

Figure 2. Representative cases at baseline and 12-month (12M) follow-up. (*Case 1*) Pure type 1 MNV. Baseline en face OCTA revealed type 1 flow only, and cross-sectional OCTA confirmed all flow signal (*yellow*) beneath the RPE (*blue dashed arrows*). At the 12-month visit, type 1 MNV component size was similar to baseline. (*Case 2*) Predominantly type 2 MNV at the baseline. En face OCTA revealed only type 2 MNV flow, and cross-sectional OCTA confirmed flow signals above the RPE (*blue dashed line*). At the 12-month visit, RPE enveloped the MNV (*red arrows*), and the type 2 component disappeared, leaving smaller residual type 1 component. (Case 3) Mixed-type MNV. En face OCTA images show type 2 component and type 1 component. Cross-sectional OCTA images show flow signals below and above the RPE (*blue dashed line*). At the 12-month visit, the type 2 component disappeared, and all flow was detected below the RPE (*blue dashed line*).

Thirteen eyes (76%) were treated with bevacizumab only, two eyes were treated with aflibercept only, and two eyes were switched from bevacizumab to aflibercept during the follow-up period.

At the baseline, 12 eyes (71%) were classified as pure type 1 MNV; type 2 MNV was identified in five eyes (29%), of which two were predominantly type 2 MNV; and three eyes were mixed type MNV, based on OCTA classification.[13] At 6-month and 12-month visits, all 17 eyes were classified as pure type 1 MNV because no type 2 MNV component was detected. In five eyes with a type 2 MNV component at the baseline, four eyes (80%) had RPE envelopment during the follow-up that converted type 2 MNV into a type 1 pattern (Fig. 2), and one eye had a complete regression of

Table 2. Changes in MNV Area and Volume Over Time

	Mean (SD) [95% CI]			*P*	
	Baseline	6 Months	12 Months	Baseline versus 6 Months	Baseline versus 12 Months
Total MNV area (mm^2)*					
All eyes ($N = 17$)	0.34 (0.26) [0.21 to 0.47]	0.35 (0.36) [0.16 to 0.53]	0.35 (0.34) [0.18 to 0.53]	0.55	0.64
Pure type 1 MNV† ($n = 12$)	0.29 (0.27) [0.12 to 0.46]	0.39 (0.42) [0.12 to 0.66]	0.37 (0.40) [0.12 to 0.63]	0.083	0.42
Type 2 MNV† ($n = 5$)	0.47 (0.21) [0.21 to 0.73]	0.25 (0.13) [0.083 to 0.42]	0.30 (0.17) [0.093 to 0.51]	0.0074‡	0.014‡
Total MNV volume (mm^3)					
All eyes ($N = 17$)	33.81 (51.7) [7.3 to 60.4]	15.7 (14.8) [8.0 to 23.3]	15.4 (13.6) [8.5 to 22.4]	0.55	0.35
Pure type 1 MNV† ($n = 12$)	10.5 (12.0) [2.9 to 18.0]	15.2 (17.0) [4.4 to 25.9]	13.3 (14.5) [4.1 to 22.6]	0.064	0.23
Type 2 MNV† ($n = 5$)	90.0 (68.7) [4.6 to 175.1]	16.9 (9.5) [5.1 to 28.7]	20.4 (10.6) [7.3 to 33.6]	0.061	0.074

* Total MNV area and volume are the sums of type 1 and type 2 vascular areas.
† MNV type was classified based on the baseline visit.
‡ Statistically significant *P* values after Bonferroni correction.

the type 2 MNV component without RPE envelopment. In terms of the types of anti-VEGF, three out of four eyes with RPE envelopment were treated with bevacizumab, and one eye was treated with 10 bevacizumab injections followed by two aflibercept injections. One eye with a type 2 MNV component that did not have an RPE envelopment was treated with 13 aflibercept injections during the follow-up period.

Overall, total MNV area, which is a sum of type 1 and type 2 area, did not change from baseline to 6 and 12 months ($P = 0.55$ and $P = 0.64$, respectively) (Table 2, Fig. 3). In the 12 eyes with pure type 1 MNV, baseline total MNV area was not statistically different than that at the 6-month visit ($P = 0.083$) or at the 12-month visit ($P = 0.42$) (Fig. 3). In contrast, in the five eyes that had a type 2 MNV component at baseline, the total MNV area was found to be significantly decreased at 6 months ($P = 0.0074$) and at 12 months ($P = 0.014$). In eyes with type 2 MNV, analysis of the separate components revealed that type 1 MNV flow area increased from 0.093 ± 0.10 mm^2 at the baseline to 0.25 ± 0.14 mm^2 at the 6-month and 12-month visits, but the increase was not statistically significant ($P = 0.071$ and $P = 0.058$, respectively) (Table 3). The baseline type 2 MNV flow area was 0.37 (0.17) mm^2 and undetectable at 6- and 12-month visits ($P = 0.0087$).

The linear mixed-effects model accounting for the number of anti-VEGF injections demonstrated a significant interaction between the baseline MNV types (reference: pure type 1 MNV) and 6-month visit (reference: baseline) for the total MNV area (estimated value = −0.079; 95% confidence interval [CI], −0.13 to −0.026; $P = 0.0062$). Also, the reduction of the MNV area at 6 months was significantly greater in eyes with a type 2 MNV component than in eyes with pure type 1 MNV. The interaction between the baseline MNV type (reference: pure type 1 MNV) and the 12-month visit (reference: baseline) for the total MNV area was also statistically significant (estimated value = −0.063; 95% CI, −0.11 to −0.016; $P = 0.012$).

Results from three-dimensional MNV volume were consistent with MNV area (Tables 2, 3; Fig. 3). The MNV flow volumes of total MNV, type 1 MNV, and type 2 MNV significantly correlated with those of the MNV flow area (all $P < 0.01$) (Table 4). In all eyes, the total MNV flow volume did not change over time (Table 2). In eyes with pure type 1, the total MNV flow volume also did not change from baseline to 6 and 12 months ($P = 0.064$ and $P = 0.23$, respectively). In eyes with type 2 MNV, total MNV flow volume at the 6- and 12-month visits decreased, with the effect nearing but not reaching statistically significant levels ($P = 0.061$ and $P = 0.074$, respectively).

Discussion

In this study, projection-resolved OCTA with a CNN-based algorithm was used to detect and quantify type 1 MNV and type 2 MNV responses to PRN anti-VEGF treatment over 1 year. This technique allows automated quantification of both MNV area and MNV volume and can be used to evaluate total MNV area and volume, isolated type 1 MNV component area and volume, and isolated type 2 MNV component area and volume. Eyes with baseline type 2 MNV showed statistically significant reduction in MNV area at 6 months and 12 months. MNV type 2 volume also decreased, with *P* values nearing statistical significance (Fig. 3, Table 2). In contrast, pure type 1 MNV area and volume did not change by a significant degree. The mixed-effects model also demonstrated that the reduction of the flow area at the 6- and 12-month visits was significantly greater in eyes with type 2 MNV than in eyes with pure type 1 MNV. These results suggest that type 2 MNV is more likely to decrease in response to anti-VEGF treatment compared to type 1 MNV.

Kim et al.[20] also reported that type 2 MNV significantly regressed compared to type 1 MNV after 1-year anti-VEGF treatment. However, Nakano et al.[28] and Levine et al.[29] reported increased type 1 and type 2 MNV size under 2-year anti-VEGF treatment. This difference may be attributed to different follow-up lengths, different anti-VEGF agents used, or different treatment protocols. In eyes with treatment-naïve exudative AMD, MNV size significantly regressed after early treatment (three loading injections),[14,30] whereas previously treated eyes did not show a significant reduction in MNV size.[30,31] The current results also showed that the MNV flow area in eyes with type 2 MNV decreased at the 6-month visit (from 0.47 mm^2 to 0.25 mm^2) followed by a trend of increasing MNV size to 0.3 mm^2. Perhaps with longer follow-up we would have detected continued increases in MNV area and volume.

Several studies prior to OCTA demonstrated varying treatment responses based on MNV types. For instance, Coscas et al.[19] found that classic MNV showed an early and sustained reduction, but Framme et al.[18] reported that occult MNV lesions typically remained stable. Our current quantitative

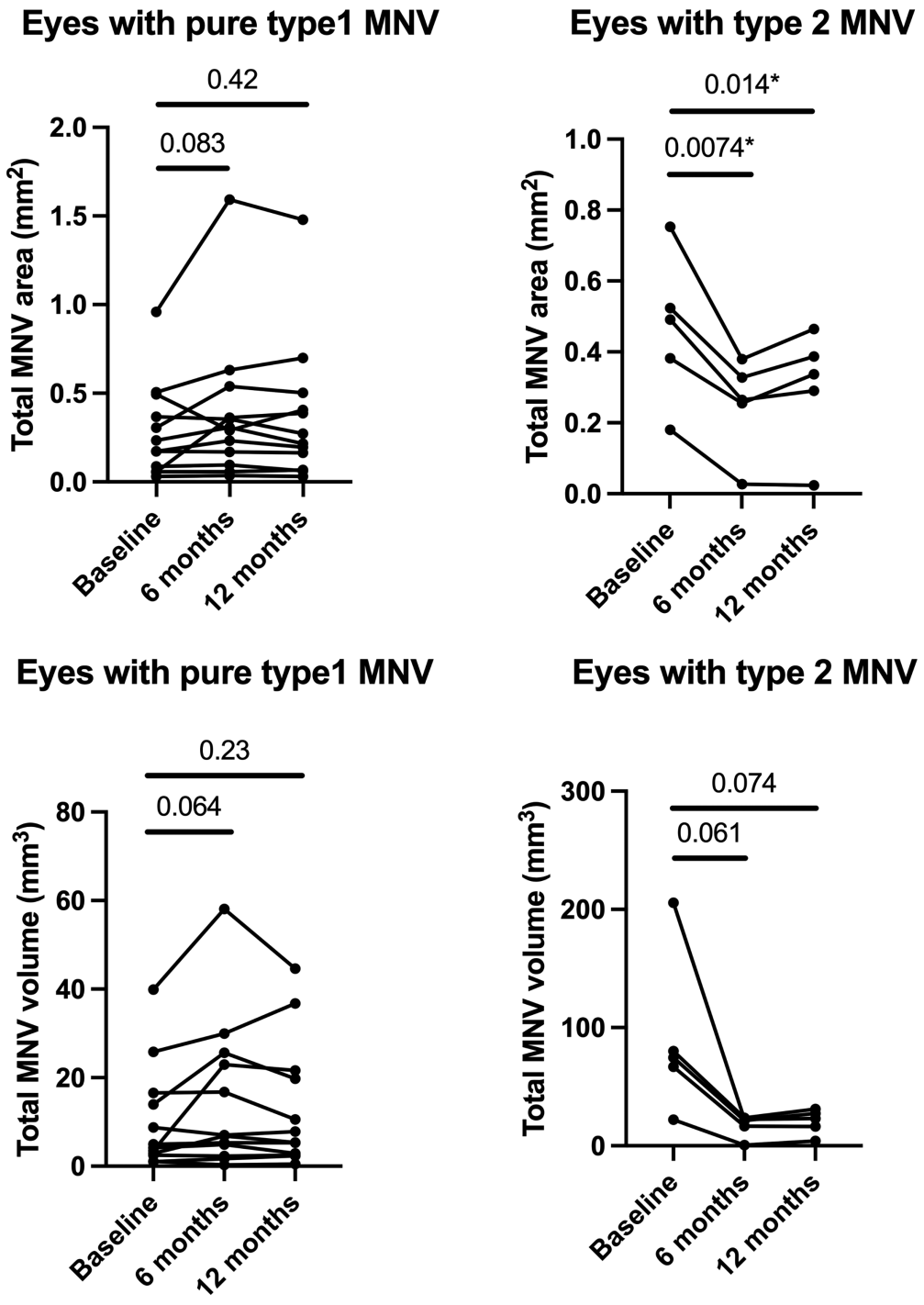

* Statistically significant P values after Bonferroni correction were noted.

Figure 3. MNV area (*upper row*) and MNV volume (*bottom row*) over 1 year under as-needed anti-VEGF treatment. Shown are the mean total MNV areas in eyes with pure type 1 MNV ($n = 12$) and eyes with type 2 MNV ($n = 5$). In pure type 1 eyes (12 eyes), mean total MNV flow area did not change at the 6-month and 12-month visits compared to the baseline visit. In eyes with a type 2 MNV component (five eyes), mean total MNV flow area decreased at the 6-month and 12-month visits compared to baseline. Similar to MNV area, MNV volume in eyes with pure type 1 MNV did not change over 1 year. In eyes with type 2 MNV, total MNV volume decreased at 6- and 12-month visits compared to baseline.

results align with these past findings. Furthermore, prior OCTA research has drawn connections between the morphological differences in the MNV vascular network and their respective treatment responses.[22,23,32–34] Kuehlewein and colleagues[32] discovered that around 75% of eyes with type 1 MNV exhibited a large mature MNV complex. In contrast, type 2 MNV appears as a branching network composed of densely packed, smaller caliber vessels.[22] Notably, type

Table 3. Change in MNV Components Under PRN Anti-VEGF Treatment in Eyes With Type 2 MNV

	Mean (SD) [95% CI]			*P*	
	Baseline	6 Months	12 Months	Baseline versus 6 Months	Baseline versus 12 Months
Type 2 MNV area (mm^2) ($n = 5$)					
Type 1 component	0.093 (0.10) [−0.03 to 0.22]	0.25 (0.14) [0.083 to 0.42]	0.30 (0.16) [0.092 to 0.51]	0.071	0.058
Type 2 component	0.37 (0.17) [0.16 to 0.59]	0	0	0.0087*	0.0087*
Type 2 MNV volume (mm^3) ($n = 5$)					
Type 1 component	4.7 (5.2) [−1.7 to 11.1]	16.9 (9.5) [5.1 to 28.7]	20.4 (10.6) [7.3 to 33.6]	0.061	0.037
Type 2 component	85.2 (70.8) [−2.7 to 173.1]	0	0	0.055	0.055

* Statistically significant *P* values after Bonferroni correction.

Table 4. Correlations Between MNV Vascular Area and MNV Flow Volume

	Baseline		6 Months		12 Months	
	*R**	*P**	*R**	*P**	*R**	*P**
Total MNV vascular area versus total MNV flow volume	0.72	0.0015	0.87	<0.0001	0.75	0.0009
Type 1 MNV vascular area versus type 1 MNV flow volume	0.88	<0.0001	0.87	<0.0001	0.75	0.0009
Type 2 MNV vascular area versus type 2 MNV flow volume	0.77	0.0003	NA†	NA†	NA†	NA†

NA, not applicable.
* Calculated based on Spearman's rank correlation coefficient.
† Type 2 MNV was not identified at 6-month and 12-month visits.

1 MNV has significantly fewer vessel junctions compared to type 2 MNV, implying that type 1 MNV is more mature and resistant to treatment than type 2 MNV.[34] Although our current study did not delve into the branching patterns and maturity levels of MNV, developing an algorithm to evaluate these morphological characteristics in type 1 and type 2 MNV might shed more light on the nature of MNV.

In this study, we applied a novel three-dimensional MNV volume analysis to assess treatment response. Two-dimensional MNV measurements may underestimate MNV size if vascular branches extend vertically or if the MNV is multilayered. However, the current results demonstrated significant correlations between the MNV area and the MNV volume. Additionally, the longitudinal changes in the MNV volume were similar to MNV area. Further study with larger sample sizes is necessary to determine if MNV volume provides added value over MNV area. In the meantime, these findings suggest that, with projection-resolved algorithms, two-dimensional analysis, such as MNV area, can capture how multilayered MNV changes over time. RPE envelopment is commonly observed in eyes with type 2 MNV treated with anti-VEGF injections.[19,35–37] In a laser-induced MNV model, RPE envelopment was observed during the MNV involutional stage.[38,39] We observed that, in all five eyes with type 2 MNV at baseline, all type 2 flow was undetectable with OCTA at 6 months and 1 year. In one case, the height of the pigment epithelial detachment (PED) decreased, and there was no evidence of new RPE formation enveloping the original type 2 MNV, suggesting that the type 2 flow completely regressed instead of being incorporated into the type 1 component. In the four other cases, the RPE enveloped the original type 2 MNV, making it difficult to separately evaluate how the original type 1 and type 2 components responded. PEDs associated with MNV have a complicated response to treatment, and PED size can vary with absorption of sub-RPE exudation, reduction in MNV tissue, and RPE expansion around type 2 MNV. Three-dimensional volumetric analysis did not help because it was impossible to register the original RPE layer height with subsequent follow-up scans. In our series of type 2 MNV, most of the baseline MNV area and MNV volume could be attributed to the type 2 MNV component (Table 3). The magnitude of the reduction of the total MNV in response to treatment is many times greater than the baseline type 1 MNV area and volume. These findings support the conclusion that MNV above the RPE is more responsive to anti-VEGF therapy than MNV below the RPE.

The current study has several limitations. A small sample size, especially the small number of eyes with type 2 MNV, limits statistical power. Because MNV is a heterogeneous disease, interpretation of the results requires caution. The current PRN treatment protocol was strictly defined as monthly visits, and any exudation was promptly treated. The type of anti-VEGF was not unified, as 76% of the eyes were treated with bevacizumab. OCTA technologies also have limitations. MNV was detected in all enrolled eyes; however, quantitative measurement of individual MNV components requires higher quality OCTA scans. In the current study, almost 30% of eyes were excluded due to the low image quality, which may lead to a selection bias. Additionally, because exudative changes reduce the signal strength,[40] MNV area and volume at baseline could have been underestimated. RPE segmentation in some cases was difficult to identify because of exudative changes, which might affect the assessment of type 1 and type 2 components, despite the two individual graders' review of the segmentations. Two study participants had both eyes enrolled, and this could bias the results. We performed a secondary analysis that randomly removed one eye from each of the participants, and our results did not change. We preferred to use 3 × 3-mm scans because of the higher sampling density and better lateral resolution compared to 6 × 6-mm scans. Five cases required

the use of 6 × 6-mm scans because the MNV extended beyond the 3 × 3-mm field of view. In these cases, it is possible that the lower sampling density could prevent detection of smaller vessels of the MNV, resulting in an underestimation of MNV changes over time. The OCTA scanning pattern used at baseline was used in all subsequent visits to ensure the follow-up data were consistent. These size constraints will become less of an issue with future OCTA scan speeds.

Despite these limitations, the current study has several strengths. The enrolled eyes were from a prospective study with strict follow-up, and the treatment protocol included only treatment-naïve cases. The distribution of MNV type based on current OCTA-based MNV classification was consistent with prior published combined FA- and OCT-based classification,[24] despite the small cohort size. In addition, the current quantitative analyses were in line with the previous findings based on the other imaging modalities. It should be noted that PR-OCTA was essential in measuring each MNV component quantitatively. OCTA allows three-dimensional analysis; however, projection artifacts produce artifactual tails that could infringe on the ability to determine MNV type. PR-OCTA now allows us to detect pathologic blood flow in the outer retina, and the combination of this with the CNN-based algorithm may integrate the conventional FA-based classification with the OCT-based classification. The potential advantages of the current method are as follows: First, automated MNV detection and measurement could be useful for quick and non-invasive monitoring of MNV management over time. For example, a high growth rate in MNV size could indicate a high risk of exudation, as already confirmed in eyes with quiescent non-exudative MNV.[41] Second, we provide evidence suggesting that there is a different treatment response between type 1 and type 2 MNV under PRN treatment with eyes primarily treated with bevacizumab at 1 year. With multiple new treatments becoming available for the treatment of exudative AMD, we can potentially use OCTA to better understand how different pharmacologic agents uniquely interact with the unique subtypes of MNV.[39]

In conclusion, we provide evidence suggesting that type 2 MNV has greater reductions in MNV area and MNV volume compared to type MNV at 6 months and 1 year under PRN anti-VEGF treatment. Although the current small study will not change current clinical management, it does demonstrate the ability to automatically quantify type 1 and type 2 MNV using OCTA. Further studies with larger sample sizes, different treatment protocols, longer follow-up, and different anti-VEGF agents may reveal useful clinical management information, provide prognostic clues, and improve our understanding of MNV pathogenesis.

Acknowledgments

Supported by grants from the National Institutes of Health (R01EY027833, R01EY024544, P30EY010572); William & Mary Greve Special Scholar Award and unrestricted departmental funding from Research to Prevent Blindness; and grants from the National Natural Science Foundation of China (81971697, 81501544). The funding source had no role in the design and conduct of the study; collection, management, analysis, and interpretation of the data; preparation, review, or approval of the manuscript; or decision to submit the manuscript for publication.

Presented at the ARVO 2021 virtual meeting.

Disclosure: **K. Tsuboi**, Alcon Japan (F), Bayer (F), Novartis Pharma (F), Santen (F); **Q.S. You**, None; **J. Wang**, None; **Y. Guo**, None; **C.J. Flaxel**, None; **T.S. Hwang**, None; **D. Huang**, Visionix/Optovue, Inc. (F, P, R), Boeringer Ingelheim Inc. (C); **Y. Jia**, Visionix/Optovue, Inc. (P, R), Genentech (P, R, F), Optos Inc. (P), Boeringer Ingelheim Inc. (C); **S.T. Bailey**, Visionix/Optovue, Inc. (F)

References

1. Ambati J, Ambati BK, Yoo SH, Ianchulev S, Adamis AP. Age-related macular degeneration: etiology, pathogenesis, and therapeutic strategies. *Surv Ophthalmol*. 2003;48(3):257–293.
2. Jager RD, Mieler WF, Miller JW. Age-related macular degeneration. *N Engl J Med*. 2008;358(24):2606–2617; published correction appears in *N Engl J Med*. 2008;359(16):1736.
3. Hee MR, Baumal CR, Puliafito CA, et al. Optical coherence tomography of age-related macular degeneration and choroidal neovascularization. *Ophthalmology*. 1996;103(8):1260–1270.
4. Grossniklaus HE, Green WR. Choroidal neovascularization. *Am J Ophthalmol*. 2004;137(3):496–503.
5. de Jong PT. Age-related macular degeneration. *N Engl J Med*. 2006;355(14):1474–1485.
6. Fine SL. Macular photocoagulation study. *Arch Ophthalmol*. 1980;98(5):832.
7. Gass JD. Biomicroscopic and histopathologic considerations regarding the feasibility of surgical excision of subfoveal neovascular membranes. *Am J Ophthalmol*. 1994;118(3):285–298.
8. Freund KB, Zweifel SA, Engelbert M. Do we need a new classification for choroidal neovascularization in age-related macular degeneration? *Retina*. 2010;30(9):1333–1349; published correction appears in *Retina*. 2011;31(1):208.
9. Jia Y, Bailey ST, Wilson DJ, et al. Quantitative optical coherence tomography angiography of choroidal neovascularization in age-related macular degeneration. *Ophthalmology*. 2014;121(7):1435–1444.
10. Jia Y, Bailey ST, Hwang TS, et al. Quantitative optical coherence tomography angiography of vascular abnormalities in the living human eye. *Proc Natl Acad Sci USA*. 2015;112(18):E2395–E2402.
11. Zhang M, Hwang TS, Campbell JP, et al. Projection-resolved optical coherence tomographic angiography. *Biomed Opt Express*. 2016;7(3):816–828.
12. Wang J, Zhang M, Hwang TS, et al. Reflectance-based projection-resolved optical coherence tomography angiography [Invited]. *Biomed Opt Express*. 2017;8(3):1536–1548.
13. Patel R, Wang J, Campbell JP, et al. Classification of choroidal neovascularization using projection-resolved optical coherence tomographic angiography. *Invest Ophthalmol Vis Sci*. 2018;59(10):4285–4291.
14. McClintic SM, Gao S, Wang J, et al. Quantitative evaluation of choroidal neovascularization under pro re nata anti-vascular endothelial growth factor therapy with OCT angiography. *Ophthalmol Retina*. 2018;2(9):931–941.
15. Liu L, Gao SS, Bailey ST, Huang D, Li D, Jia Y. Automated choroidal neovascularization detection algorithm for optical coherence tomography angiography. *Biomed Opt Express*. 2015;6(9):3564–3576.
16. Wang J, Hormel TT, Gao L, et al. Automated diagnosis and segmentation of choroidal neovascularization in OCT angiography using deep learning. *Biomed Opt Express*. 2020;11(2):927–944.
17. Tsuboi K, You QS, Guo Y, et al. Association between fluid volume in inner nuclear layer and visual acuity in diabetic macular edema. *Am J Ophthalmol*. 2022;237:164–172.

18. Framme C, Panagakis G, Birngruber R. Effects on choroidal neovascularization after anti-VEGF upload using intravitreal ranibizumab, as determined by spectral domain-optical coherence tomography. *Invest Ophthalmol Vis Sci*. 2010;51(3):1671–1676.
19. Coscas F, Querques G, Forte R, Terrada C, Coscas G, Souied EH. Combined fluorescein angiography and spectral-domain optical coherence tomography imaging of classic choroidal neovascularization secondary to age-related macular degeneration before and after intravitreal ranibizumab injections. *Retina*. 2012;32(6):1069–1076.
20. Kim JM, Cho HJ, Kim Y, Jung SH, Lee DW, Kim JW. Responses of types 1 and 2 neovascularization in age-related macular degeneration to anti-vascular endothelial growth factor treatment: optical coherence tomography angiography analysis. *Semin Ophthalmol*. 2019;34(3):168–176.
21. Nesper PL, Soetikno BT, Treister AD, Fawzi AA. Volume-rendered projection-resolved OCT angiography: 3D lesion complexity is associated with therapy response in wet age-related macular degeneration. *Invest Ophthalmol Vis Sci*. 2018;59(5):1944–1952.
22. Kuehlewein L, Sadda SR, Sarraf D. OCT angiography and sequential quantitative analysis of type 2 neovascularization after ranibizumab therapy. *Eye (Lond)*. 2015;29(7):932–935.
23. Coscas GJ, Lupidi M, Coscas F, Cagini C, Souied EH. Optical coherence tomography angiography versus traditional multimodal imaging in assessing the activity of exudative age-related macular degeneration: a new diagnostic challenge. *Retina*. 2015;35(11):2219–2228.
24. Jung JJ, Chen CY, Mrejen S, et al. The incidence of neovascular subtypes in newly diagnosed neovascular age-related macular degeneration. *Am J Ophthalmol*. 2014;158(4):769–779.e2.
25. Cohen SY, Creuzot-Garcher C, Darmon J, et al. Types of choroidal neovascularisation in newly diagnosed exudative age-related macular degeneration. *Br J Ophthalmol*. 2007;91(9):1173–1176.
26. Zhang M, Wang J, Pechauer AD, et al. Advanced image processing for optical coherence tomographic angiography of macular diseases. *Biomed Opt Express*. 2015;6(12):4661–4675.
27. Bennett AG, Rudnicka AR, Edgar DF. Improvements on Littmann's method of determining the size of retinal features by fundus photography. *Graefes Arch Clin Exp Ophthalmol*. 1994;232(6):361–367.
28. Nakano Y, Takeuchi J, Horiguchi E, et al. Long-term morphologic changes in macular neovascularization under aflibercept treatment with a treat-and-extend regimen. *Retina*. 2023;43(3):412–419.
29. Levine ES, Custo Greig E, Mendonça LSM, et al. The long-term effects of anti-vascular endothelial growth factor therapy on the optical coherence tomography angiographic appearance of neovascularization in age-related macular degeneration. *Int J Retina Vitreous*. 2020;6:39.
30. Miere A, Oubraham H, Amoroso F, et al. Optical coherence tomography angiography to distinguish changes of choroidal neovascularization after anti-VEGF therapy: monthly loading dose versus pro re nata regimen. *J Ophthalmol*. 2018;2018:3751702.
31. Al-Sheikh M, Iafe NA, Phasukkijwatana N, Sadda SR, Sarraf D. Biomarkers of neovascular activity in age-related macular degeneration using optical coherence tomography angiography. *Retina*. 2018;38(2):220–230.
32. Kuehlewein L, Bansal M, Lenis TL, et al. Optical coherence tomography angiography of type 1 neovascularization in age-related macular degeneration. *Am J Ophthalmol*. 2015;160(4):739–748.e2.
33. Spaide RF. Optical coherence tomography angiography signs of vascular abnormalization with antiangiogenic therapy for choroidal neovascularization. *Am J Ophthalmol*. 2015;160(1):6–16.
34. Nakano Y, Kataoka K, Takeuchi J, et al. Vascular maturity of type 1 and type 2 choroidal neovascularization evaluated by optical coherence tomography angiography. *PLoS One*. 2019;14(4):e0216304.
35. Toju R, Iida T, Sekiryu T, Saito M, Maruko I, Kano M. Near-infrared autofluorescence in patients with idiopathic submacular choroidal neovascularization. *Am J Ophthalmol*. 2012;153(2):314–319.
36. Dolz-Marco R, Phasukkijwatana N, Sarraf D, Freund KB. Regression of type 2 neovascularization into a type 1 pattern after intravitreal anti-vascular endothelial growth factor therapy for neovascular age-related macular degeneration. *Retina*. 2017;37(2):222–233.
37. Chen L, Li M, Messinger JD, Ferrara D, Curcio CA, Freund KB. Recognizing atrophy and mixed-type neovascularization in age-related macular degeneration via clinicopathologic correlation. *Transl Vis Sci Technol*. 2020;9(8):8.
38. Miller H, Miller B, Ryan SJ. The role of retinal pigment epithelium in the involution of subretinal neovascularization. *Invest Ophthalmol Vis Sci*. 1986;27(11):1644–1652.
39. Iida T, Hagimura N, Kishi S, Shimizu K. Indocyanine green angiographic features of idiopathic submacular choroidal neovascularization. *Am J Ophthalmol*. 1998;126(1):70–76.
40. Yu JJ, Camino A, Liu L, et al. Signal strength reduction effects in OCT angiography. *Ophthalmol Retina*. 2019;3(10):835–842.
41. Bailey ST, Thaware O, Wang J, et al. Detection of nonexudative choroidal neovascularization and progression to exudative choroidal neovascularization using OCT angiography. *Ophthalmol Retina*. 2019;3(8):629–636.

Investigative Ophthalmology & Visual Science